Review

Applications of Artificial Intelligence and Radiomics in Molecular Hybrid Imaging and Theragnostics for Neuro-Endocrine Neoplasms (NENs)

Michele Balma[1]*, Riccardo Laudicella[2], Elena Gallio[3], Sara Gusella[4], Leda Lorenzon[5], Simona Peano[1], Renato P. Costa[2], Osvaldo Rampado[3], Mohsen Farsad[4], Laura Evangelista[6], Désirée Deandreis[7], Alberto Papaleo[1] and Virginia Liberini[1]

1 Nuclear Medicine Department, S. Croce e Carle Hospital, 12100 Cuneo, Italy. balma.m@ospedale.cuneo.it; peano.s@ospedale.cuneo.it; papaleo.a@ospedale.cuneo.it; liberini.v@ospedale.cuneo.it;
2 Unit of Nuclear Medicine, Biomedical Department of Internal and Specialist Medicine, University of Palermo, Palermo, Italy. riclaudi@hotmail.it; renatopatrizio.costa@policlinico.pa.it;
3 Medical Physics Unit, A.O.U. Città Della Salute E Della Scienza Di Torino, Corso Bramante 88/90, 10126, Torino, Italy. egallio@cittadellasalute.to.it; orampado@cittadellasalute.to.it;
4 Nuclear Medicine, Central Hospital Bolzano, 39100 Bolzano, Italy. sara.gusella@sabes.it; mohsen.farsad@sabes.it;
5 Medical Physics Department, Central Bolzano Hospital, 39100 Bolzano, Italy. leda.lorenzon@sabes.it;
6 Department of Biomedical Sciences, Humanitas University, 20089 Pieve Emanuele-Milan, Italy. med.evangelista.laura@gmail.com;
7 Department of Nuclear Medicine and Endocrine Oncology, Gustave Roussy and Université Paris Saclay, 94805 Villejuif, France. desiree.DEANDREIS@gustaveroussy.fr
* Correspondence: mitch.balma@gmail.com; balma.m@ospedale.cuneo.it; Tel.: 0171641734

Simple Summary: Neuroendocrine neoplasms (NEN) are rare and heterogeneous tumors that often require multidisciplinary evaluation for proper diagnosis and clinical management. In this context, positron emission tomography/computed tomography (PET/CT) plays an important role in allowing disease extension, evaluating the 'in vivo' expression of somatostatin receptors (SSTRs) through [^{68}Ga]Ga-DOTA-labelled somatostatin analogs, and tumor metabolism in more aggressive tumors through [^{18}F]FDG. More recently, it has been possible to increase the information retrievable from the analysis of PET/CT images using mathematical algorithms (radiomics) and artificial intelligence. This systematic review aims to summarize the most recent research on radiomics and AI used for molecular imaging of NENs.

Abstract: Nuclear medicine has acquired a crucial role in the management of patients with neuroendocrine neoplasms (NENs) by improving the accuracy of diagnosis and staging, their risk stratification and personalized therapies, including radioligand therapies (RLT). Artificial intelligence (AI) and radiomics can enable physicians to further improve the overall efficiency and accuracy of the use of these tools in both diagnostic and therapeutic settings by improving the prediction of tumor grade, differential diagnosis from other malignancies, assessment of tumor behavior and aggressiveness, and prediction of treatment response. This systematic review aims to describe the state-of-the-art on AI and radiomics applications in molecular imaging of NENs.

Keywords: neuroendocrine tumor; NET; machine-learning; nuclear medicine; theragnostics; PET; DOTA PET; radiomics

1. Introduction

Neuroendocrine neoplasms (NENs) comprise a wide variety of heterogeneous tumors, originating from the diffuse neuroendocrine system. These tumors are considered rare, with an incidence of about 3-5 new cases/100,000 inhabitants/year, although new data from the *US Surveillance Epidemiology and End Results Program (SEER)* show an increase in the incidence of the disease of about 520% over the last 32 years (1973-2005), with an annual rate of 5.8% [1]. This increase in incidence can be partially attributed to the introduction of new and/or more sophisticated diagnostic tools, such as single-photon emission computed tomography (SPECT), positron emission tomography (PET) combined with computed tomography (PET/CT) or magnetic resonance imaging (PET/MRI).

 doi:10.20944/preprints202306.0677.v1

Although ubiquitous, these tumors most frequently affect the gastro-entero-pancreatic (GEP) tract (33%), and the bronchopulmonary system (25%). The survival of NET depends on the site, and the stage according to the 2022 Tumor, Node, Metastasis (TNM) classification and the World Health Organization (WHO) histopathological classification, which expresses both the morphological appearance of the tumor and its proliferative activity in terms of the number of mitoses and proliferation index (by assessing the Ki-67 index and thus the disease grading) [2,3]. The current WHO classification of neuroendocrine tumors is given in Table 1.

Preprints (www.preprints.org) | NOT PEER-REVIEWED | Posted: 9 June 2023 doi:10.20944/preprints202306.0677.v1

Table 1. The World Health Organization (WHO) 2022 classification of neuroendocrine neoplasms.

	Lung and thymus	***Mitotic Index***	***Necrosis***	***Other features***	**Gastro-intestinal (GI) tract and hepatopancreatobiliary organs**	***Mitotic Index***	***Ki67 Index***	***Other features***	**Upper aerodigestive tract and salivary glands**	***Mitotic Index***	***Ki67 Index***	***Other features***	**Thyroid**	***Mitotic Index***	***Ki67 Index***	***Necrosis***
Well-differentiated *	NET, TC	<2/10HPF	No		NET, G1	<2/10HPF	<3%		NET. G1	<2/10HPF	<20%		Low grade MTC	<5/10HPF	<5%	No
	NET, AC	2-10/10HPF	Yes (punctate)		NET, G2	2–20/10HPF	3-20%		NET. G2	2–10/10HPF	<20%					
	Carcinoids/NETs	>10/10HPF	Yes	and/or Ki67 index (>30%)	NET, G3	>20/10HPF	>20%		NET, G3	>10/10HPF	>20%					
Poorly differentiated *	NEC, SCLC	>10/10HPF	Yes	small cell cytomorphology	NEC, SCNEC	>20/10HPF	>20% (often >70%)	small cell cytomorphology	NEC, SCNEC	>20/10HPF	>20% (often >70%)	small cell cytomorphology	High grade MTC	>/10HPF	>5%	Yes
	NEC, LCNEC	>10/10HPF	Yes	large cell cytomorphology	NEC, LCNEC	>20/10HPF	>20% (often >70%)	large cell cytomorphology	NEC, LCNEC	>20/10HPF	>20% (often >55%)	large cell cytomorphology				
Mixed neoplasms	MiNENs	NA	>30%		MiNENs	NA	>30%		MiNENs	NA	>30%					

NOTE: *AC* atypical carcinoid, *HPF* high-power field, *LCNEC* large cell neuroendocrine carcinoma, *MiNEN* mixed neuroendocrine/non-neuroendocrine neoplasm, *MTC* medullary thyroid carcinomas, *NEC* neuroendocrine carcinoma, *NET* neuroendocrine tumor, *SCLC* small-cell lung carcinoma, *SCNEC* small cell neuroendocrine carcinoma, *TC* typical carcinoid,

**Morphologically well-differentiated or poorly differentiated*

Preprints (www.preprints.org) | NOT PEER-REVIEWED | Posted: 9 June 2023 doi:10.20944/preprints202306.0677.v1

Further prognostic factors are chromogranin A (CgA), synaptophysin, somatostatin receptor (SSTRs) expression, the tumor's spontaneous evolution speed, and the patient's age [4,5]. Among these, the expression of somatostatin receptors (SSTRs) is one of the most remarkable features of well-differentiated tumors, SSTRs type 1 and type 2 are present in most NENs [6].

In-vivo imaging of SSTR expression in NENs is feasible with both [^{111}In]DTPA-octreotide scintigraphy (Octreoscan®) SPECT and somatostatin analog PET, such as [^{68}Ga]Ga-DOTANOC, [^{68}Ga]Ga-DOTATATE, and [^{68}Ga]Ga-DOTATOC [7,8]. These radiotracers are commonly used for the study of well-differentiated NENs (G1 and G2 with low-intermediate levels of the Ki-67 index, <10%). Differently, in case of high levels of Ki-67 index (>10%), high-grade NET (G3), NEC, or in case of [^{68}Ga]Ga-DOTA-peptide imaging of SSTR-negative lesions, patients are also candidates for [^{18}F]FDG PET/CT, a glucose analog in which a fluorine atom replaces the OH group at position 2 [9–12]. NENs usually are growing slowly with a low rate of glucose metabolism, indeed [^{18}F]FDG PET/CT scans are more likely to detect more aggressive and poor-differentiated NENs, which are correlates to a worse clinical outcome. [13].

In 2017, Chan et al. [14] proposed a staging protocol by means of [^{18}F]FDG and [^{68}Ga]Ga-DOTA-peptides PET/CT, resulting in the formulation of a new score, the "NETPET grade", which could help in the prognostic evaluation of NEN patient and the resulting therapeutic decisions. However, to date, this protocol is hardly applicable in the clinical setting: imaging with multiple radiotracers, although potentially providing the most accurate biological characterization of the disease, is not feasible/reimbursed in all patients and should only be considered in selected cases.

This drawback might be partially solved using new artificial intelligence (AI) approaches to extract data from both [^{68}Ga]Ga-DOTA-labelled somatostatin analogs and/or [^{18}F]FDG PET/CT images [15–19]. Indeed, radiomics uses bioinformatics and data-characterization algorithms to extract several quantitative characteristics (features) from medical images. These characteristics, known as radiomics features (RFs), may be able to identify disease characteristics that are invisible to the human eye, opening the door to the prospect of quantifying particular tumor characteristics and phenotypes [20,21]. There are a large number of radiomic features, related to morphological properties, the intensity distributions of the image voxels, or to the properties of the image texture. Standardized definitions of principal RFs are provided in the reference manual of the Imaging Biomarker Standardization Initiative (IBSI) [22,23]. According to the EANM/SNMMI guidelines on radiomics in nuclear medicine [24], there are three categories of radiomics-based approaches: hand-crafted radiomics (with explicit extraction of pre-designed radiomics features from the images followed by univariate or multivariate analysis), representation-learning based radiomics (with automatic discovering of features and patterns inherent in the images) and hybrid radiomics (a combination of the two other frameworks), AI comprises different types of algorithms that can perform complex tasks by learning from available data, similar to human intelligence. Under the general category of "AI", deep learning (DL), reinforcement learning, supervised machine learning, and unsupervised machine learning are all included [25–29].

Nuclear medical imaging provides indispensable information for staging, monitoring, and treatment choice and the application of new radiomics and AI tools could implement the information extracted from PET/CT imaging in each setting. This systematic review aims to summarize the most recent research on radiomics and AI used for molecular imaging of NENs.

2. Materials and Methods

We searched the PubMed, PMC, Scopus, Google Scholar, Embase, Web of Science, and Cochrane library databases (between January 2010 and May 2023), using the following, both as text and as MeSH terms: “neuroendocrine tumor*”, "NET*", “NEN*”, “artificial intelligence”, “machine learning”, “deep learning”, “convolutional neural network”, “artificial neural network”, “radiomic”, “segmentation”, “PET”, “PET/CT”, “PET/MR”, “octreotide”, “[^{68}Ga]Ga-DOTATOC”, “[^{68}Ga]Ga-DOTANOC”, “[^{68}Ga]Ga-DOTATATE”, “FDG”, “[^{18}F]Fluorodeoxyglucose, “DOPA”, “[^{177}Lu]Lu”, “[^{90}Y]Y”, “diagnosis”, “screening”, “theranostic”, “theragnostic”, “RLT”, “PRRT” and “peptide receptor radionuclide therapy”. No language restriction was applied to the search, but only articles in English were reviewed. The comprehensive literature review produced 84 papers. After removing duplicates in accordance with the Preferred Reporting Items for Systematic Review and Metanalysis (PRISMA) criteria, 25 papers have been taken into consideration, reviewed, examined, and in-depth detailed in accordance with their title and abstract as previously stated [30]. We also looked for more pertinent articles in the articles' references that were part of the retrieved literature. Following that, articles were divided into clinical and technical applications. Figure 2 provides a graphic illustration of the search and review strategy.

Preprints (www.preprints.org) | NOT PEER-REVIEWED | Posted: 9 June 2023 doi:10.20944/preprints202306.0677.v1

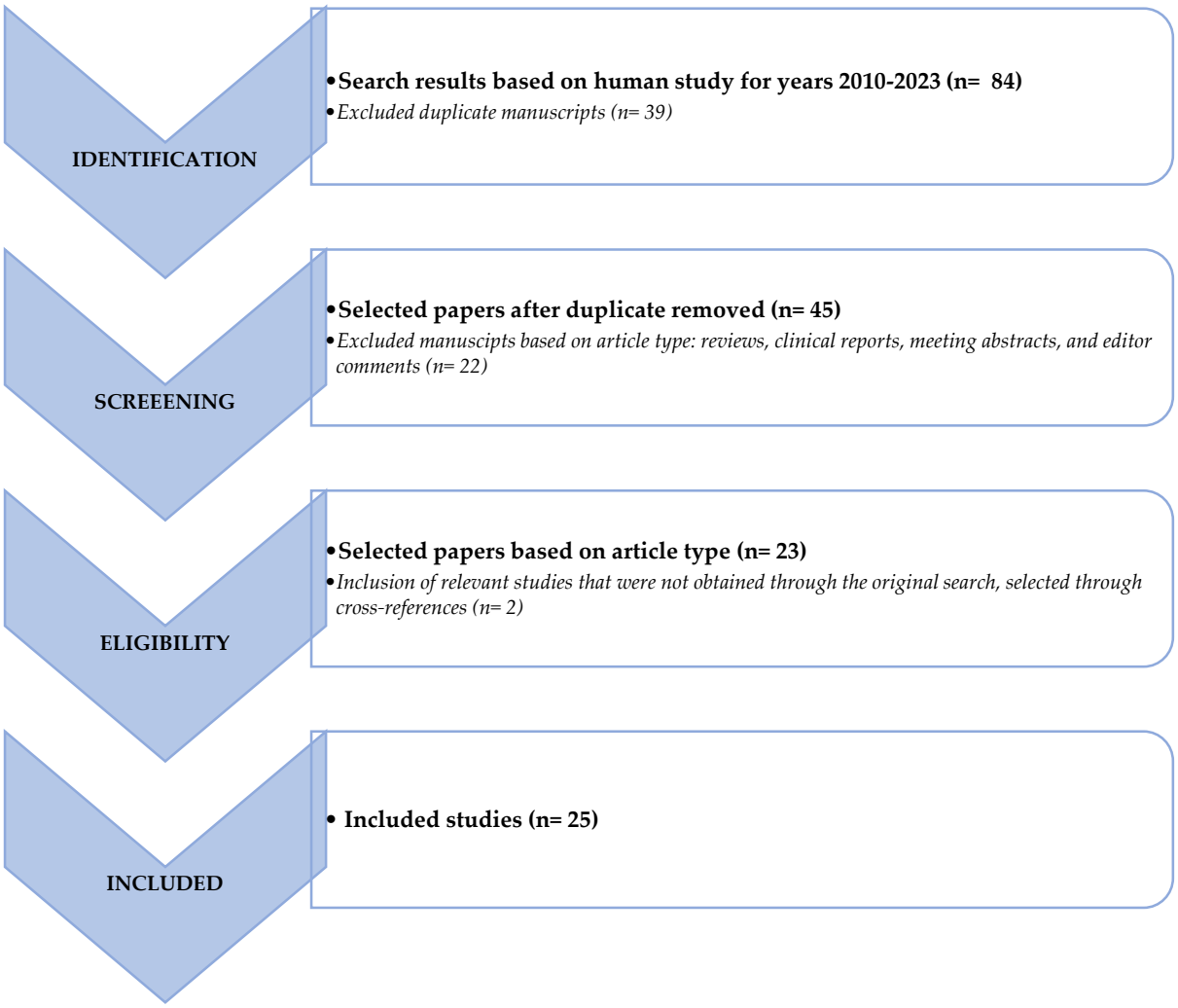

Figure 2. Schematic representation of the performed literature search and the review strategy.

3. Clinical Applications

As aforementioned, nuclear medicine plays a crucial role in the non-invasive assessment of NET for staging, treatment response assessment, and RLT eligibility evaluation; all of these can be enhanced by radiomics and AI.

3.1. Staging

The prognosis of NEN is strongly related to histologic subtypes, the correct identification of which is crucial in decision-making. The high diagnostic performance of dual [^{18}F]FDG and [^{68}Ga]DOTA-peptides PET/CT imaging for the detection of intra-tumor heterogeneity is now well known, facilitating the identification of the most aggressive tumor and the best target lesions for diagnostic biopsy [2,14,31]. In this context, RFs extraction from PET/CT images could further improve the characterization of histologic patterns and the prognosis of NEN lesions.

Already in 2017, Giesel et al. [32] published a study on the correlation between SUV_{max} and CT radiomics analysis using lymph node density in the CT component of the PET/CT examination to differentiate malignant from benign lymph nodes. The authors used a sample size of 1,022 lymph nodes extracted from the PET/CT examinations of 148 patients with different tumor types: 327 lymph nodes from 40 patients with lung cancer; 224 lymph nodes from 33 patients with malignant melanoma; 217 lymph nodes from 35 patients with GEP-NET; 254 lymph nodes from 40 patients with prostate cancer. Despite the large heterogeneity of the population evaluated, in terms of pathology and PET radiopharmaceutical analysis ([^{18}F]FDG, [^{68}Ga]Ga-DOTATOC, and [^{68}Ga]Ga-PSMA-11), the study showed that PET-

Preprints (www.preprints.org) | NOT PEER-REVIEWED | Posted: 9 June 2023 doi:10.20944/preprints202306.0677.v1

positive lymph nodes had significantly higher CT densities than PET-negative ones, irrespective of the type of cancer, identifying a CT density threshold of 7.5 Hounsfield units to differentiate between malignant and benign infiltration of lymph nodes and 20 Hounsfield units to exclude benign lymph nodes processes.

In 2020, Weber et al. [33], sought to determine whether conventional PET and MRI parameters and RFs derived from simultaneous [^{68}Ga]Ga-DOTATOC PET/CT and MRI were related to the proliferative activity of NETs, potentially allowing for a non-invasive tumor grading. The authors evaluated 304 lesions from 100 NET/NECs patients. They showed that differences between G1 and G2 tumors in conventional PET parameters, MRI ADC values, and RFs determined from both modalities were statistically significant. However, the correlation between the aforementioned parameters and Ki-67-index was weak, suggesting that RFs extracted from combined PET/MRI may not be reliably used for accurate non-invasive tumor grading in patients with Ki-67 < 30%. Further insights have been presented by Thuillier et al. [34] who assessed if conventional PET parameters and RFs extracted by [^{18}F]FDG PET/CT could differentiate among different histological subtypes (NETs vs NECs) of lung-NENs in forty-four naïve-treatment patients (15 TC, 11 AC, 1 TC or AC, 16 LCNEC and 3 SCLC). Namely, conventional PET parameters resulted to be able to distinguish Lu-NECs from Lu-NETs (SUV_{max} cut-off = 5.16; AUC = 0.91; $p < 0.001$), but not TC from AC. In fact, stratifying TC and AC according to Ki-67 level, SUV_{max} and SUV_{mean} showed a positive correlation with Ki-67, without statistical significance ($p = 0.05$ and 0.07, respectively). Regarding the TNM status, SUV_{max}, MTV, and TLG of the primary lesion were significantly associated with N+ status ($p < 0.05$). On the contrary, RFs did not provide additional information.

More recently, Fonti et al. [35] aimed to test the ability of the coefficient of variation (CoV) derived from [^{68}Ga]DOTA-peptides PET/CT imaging in the evaluation and quantification of the heterogeneity of SSTR2 expression within 107 tumor lesions (including 35 primary tumors, 32 metastatic lymph nodes, and 40 distant metastases) of 38 NENs patients (25 GEP-NENs, 7 lung-NENs and 6 from other anatomic districts). Among the RFs for the assessment of tumor heterogeneity, CoV is a simple first-order parameter that indicates the percent variability of SUV_{mean} within the tumor volume reflecting the heterogeneity of tracer distribution. Average CoVs were 0.49 ± 0.20 for primary tumors, 0.57 ± 0.26 for lymph node metastases, and 0.44 ± 0.20 for distant metastases. The CoVs of malignant lesions were up to 4-fold higher than those of normal tissues ($P \leq 0.0001$). Among malignant lesions, the highest CoV was found for bone metastases (0.68 ± 0.20), and it was significantly greater than that of primary lesions ($p = 0.01$) and liver metastases ($p < 0.0001$). The lowest CoV was observed for liver lesions (0.32 ± 0.07), probably because of the high background uptake. On the other hand, no statistically significant differences were found between the SUV_{max} of primary lesions, lymph node metastases and distant metastases, although the SUV_{max} of distant metastases tended to be higher than that of primary lesions ($p = 0.0573$).

Three studies focused on evaluating the role of radiomics parameters extracted by [^{68}Ga]DOTA-peptides PET images in predicting histopathological prognostic factors in pancreatic NEN tumors (PanNETs) patients. In 2020, Mapelli et al. [36] retrospectively extracted conventional and tumor burden PET parameters and radiomics parameters (using Chang-Gung Image Texture Analysis software package, version 1.3; digitalisation method: 4; digitalisation bins: 64) on the primary tumor lesion from both [^{18}F]FDG and [^{68}Ga]Ga-DOTATOC PET/CT scan images of 61 treatment-naive PanNET patients undergoing surgery. Intensity variability, SZV, homogeneity, SUV_{max} and MTV were predictive for tumor dimension in [^{18}F]FDG images. From principal component analysis (PCA), 4 elements were extracted: PC1 correlated with all [^{18}F]FDG variables, while PC2, PC3 and PC4 with [^{68}Ga]Ga-DOTATOC variables. The only significant predictor of angioinvasion was PC1 ($p = 0.02$), while the only significant predictor of lymph node involvement was PC4 ($p = 0.015$). All principal components except PC4 significantly predicted tumor dimension ($p < 0.0001$ for PC1, $P = 0.0016$ for PC2 and $p < 0.0001$ for PC3). The same group [37] extracted conventional PET and MRI parameters, and radiomics parameters from hybrid [^{68}Ga]Ga-DOTATOC PET/MRI of 16 treatment-naive PanNET patients undergoing surgery, using another open-source Python package Pyradiomics 3.0.1 (https:// www.radiomics.io/pyradiomics.html). They discovered a moderately significant, inverse connection (rho = 0.58, p = 0.02) between SUVmax and LN involvement. SUVmax proved to be a reliable indicator of LN involvement, with an AUC of 0.850 (95% CI: 0.60-1.00), an optimal cut-off value of 90.960, sensitivity of 60%, and specificity of 100%. Potential correlations between radiomics characteristics and tumor grade, LN involvement and vascular invasion were analyzed. After adjustment for multiple comparisons, only second-order radiomics parameters Gray-Level-Variance (GLV) and High-Gray-Level-Zone-Emphasis (HGLZE) extracted from T2 MRI demonstrated significant correlations with LN involvement (adjusted p = 0.009), also showing a good predictive performance (AUC = 0.992), with an optimal cut-off value of 0.145 for GLV (correspondent sensitivity and specificity of 90% and 100%, respectively) and of 1.545 for HGLZE (correspondent sensitivity and specificity of 90% and 100%, respectively). Finally, Bevilacqua et al. [38] extracted conventional PET and

 doi:10.20944/preprints202306.0677.v1

radiomics parameters from [^{68}Ga]Ga-DOTANOC PET/CT imaging of 51 patients with primary G1-G2 treatment-naive PanNET to investigate their ability to predict G1 versus G2 patients . Patients were grouped according to the method of tumor grade assessment: histology on the entire primary excised lesion (HS) or biopsy (BS). Three radiomics models were evaluated: A (trained on HS, validated on BS), B (trained on BS, validated on HS) and C (using cross-validation on the entire dataset). HS group SUV_{max} values did not significantly differ between G1 (36.9 ± 23.5, [6.9–84.8]) and G2 (45.3 ± 28.6, [15.0–95.7]) (p-value = 0.60). On the contrary, the grade of the primary lesion was accurately determined when using RFs: the best RF pairs for predicting G2 and G1 were second-order normalized homogeneity and entropy (p-value = 0.0002 with AUC = 0.94 (95% CI, 0.74-0.99). Model A had the best performance (test AUC = 0.90, sensitivity = 0.88, specificity = 0.89) whereas Model C had the worst performance (test median AUC = 0.87, sensitivity = 0.83, specificity = 0.82).

In 2022, Noortman et al. [39] investigated the use of [^{18}F]FDG-PET/CT radiomics, SUV_{max}, and biochemical profile for the identification of the genetic clusters of 40 paragangliomas (PPGLs) patients (13 cluster 1, 18 cluster 2, 9 sporadic). The dataset was split into five equal-sized folds, stratified for the genetic clusters. Each subgroup consecutively served as a test set and the remaining four-fifths of patients served as the training set. The biochemical profile alone was the lowest performing model with an average multiclass AUC of 0.60. The three-factor PET model showed the best classification performance to distinguish cluster 1 from cluster 2 of PPGL (multiclass AUC of 0.88), however comparable to the performance achieved by SUV_{max} alone (multiclass AUC of 0.85), which could therefore be preferred to the radiomics analysis model in a clinical scenario being more handleable. The most important characteristics and results of the above-mentioned studies are summarized in Table 2.

Preprints (www.preprints.org) | NOT PEER-REVIEWED | Posted: 9 June 2023 doi:10.20944/preprints202306.0677.v1

Table 2. Published articles concerning the implementation of radiomic and/or AI tools in the staging of NEN patients.

Author	Year of Publication	Study Design	NET Type	Number of patients	Source of data	Software	AI application	Validation	Findings
Giesel et al. [58]	2017	retrospective	GEP-NET	35	[^{68}Ga]DOTA-peptides PET/CT	software developed at the Fraunhofer Institute for Medical Image Computing	No	No	PET-positive lymph nodes had significantly higher CT densities than PET-negative ones, irrespective of the type of cancer
Weber et al. [59]	2020	retrospective	all NENs	100	[^{68}Ga]DOTA-peptides PET/MRI	LIFEx	No	No	the correlation between imaging parameters (conventional PET parameters, ADC values from MRI, and RFs parameters) and Ki-67-index was weak
Thuillier et al. [60]	2020	retrospective	Lung-NET	44	[^{18}F]FDG PET/CT	LIFEx	No	No	conventional PET parameters resulted to be able to distinguish Lu-NECs from Lu-NETs, but not TC from AC. On the contrary, RFs did not provide additional information
Fonti et al. [61]	2022	retrospective	all NENs	38	[^{68}Ga]DOTA-peptides PET/CT	LIFEx	No	No	The CoVs of malignant lesions were up to 4-fold higher than those of normal tissues ($P \leq 0.0001$)
Mapelli et al. [62]	2020	retrospective	Pan-NENs	61	[^{68}Ga]DOTA-peptides and [^{18}F]FDG PET/CT	Chang-Gung Image Texture Analysis software package	No	No	Intensity variability, SZV, homogeneity, SUV_{max} and MTV were predictive for tumor dimension in [^{18}F]FDG images. All principal components except PC4 significantly predicted tumor dimension ($p < 0.0001$ for PC1, P =

Preprints (www.preprints.org) | NOT PEER-REVIEWED | Posted: 9 June 2023 doi:10.20944/preprints202306.0677.v1

									0.0016 for PC2 and p < 0.0001 for PC3).
Mapelli et al. [63]	2022	retrospective	Pan-NENs	16	[^{68}Ga]DOTA-peptides PET/MRI	Python package Pyradiomics 3.0.1	No	No	a significant inverse correlation between SUV_{max} and LN involvement (rho = − 0.58, p = 0.02). Only second-order GLV and HGLZE extracted from T2 MRI demonstrated significant correlations with LN involvement (adjusted p = 0.009)
Bevilacqua et al. [64]	2021	retrospective	Pan-NENs	51	[^{68}Ga]DOTA-peptides PET/TC	ImageJ and MATLAB®	No	Yes	SUV_{max} values did not significantly differ between G1 and G2 (p-value = 0.60). On the contrary, the primary lesion's grade was correctly identified when using RFs, second-order normalized homogeneity and entropy (p-value = 0.0002 with AUC = 0.94)
Noortman et al. [65]	2022	retrospective	PPGLs	40	[^{18}F]FDG-PET/CT	Python package Pyradiomics 3.0.1	No	Yes	the three-factor PET model showed the best classification performance to distinguish cluster 1 from cluster 2 of PPGL (multiclass AUC of 0.88), however comparable to the performance achieved by SUV_{max} alone (multiclass AUC of 0.85)

Preprints (www.preprints.org) | NOT PEER-REVIEWED | Posted: 9 June 2023 doi:10.20944/preprints202306.0677.v1

3.2. Restaging

The use of PET, CT, MRI, and SPECT data as potential prognostic biomarkers for therapy response may benefit from the application of radiomics and AI. Targeted therapies, such as RLT, may be significantly impacted by these techniques. Numerous radiomics features have been shown to be related to tumor heterogeneity and may be able to forecast biological behavior and tumoral aggressiveness, which will enable patient-tailored treatments [19,40–42]. For monitoring and evaluating treatment response in NETs patients, several radiomics and AI studies have already been published.

In 2017, Nogueira et al. [43] developed an artificial neural networks (ANN) approach to automatically assess the treatment response of patients suffering from NENs (34 patients) and Hodgkyn lymphoma (29 patients), based on image features extracted from pre- and post-treatment [^{18}F]FDG and [^{68}Ga]Ga-DOTANOC PET/CT scans, respectively. Cases were divided into four classes of treatment response – negative (malignancy increased), neutral (no response), positive incomplete (malignancy decreased but lesion did not disappear), and positive complete (the lesion disappeared). Four standard ANN architectures were explored: multilayer perceptron (MLP), radial basis function neural network (RBFNN), probabilistic neural network (PNN) and learning vector quantization neural network (LVQNN). After synthetic data generation and PCA-based dimensionality reduction to only two components, LVQNN assured classification accuracies of 100%, 100%, 96.3%, and 100% regarding the 4 response-to-treatment classes.

In 2016, Wetz et al. [44] compared the Krenning score, tumor/lesion (T/L) ratio and asphericity (ASP) between responding and non-responding lesions (total n = 66) segmented on baseline [^{111}In]DTPA-octreotide scintigraphy (Octreoscan®) SPECT. According to their analysis, a greater ASP level was related to a worse response to RLT. Additionally, ASP outperformed both the Krenning score and the T/L ratio being the parameter with the greatest AUC (> 0.96) at 4 and 12 months of follow-up to distinguish responding from non-responding lesions. In 2020, the same group [45] evaluated the lesional asphericity (ASP), extracted from the pre-therapeutic Octreoscan, as the first imaging-based prognostic marker for progression-free survival (PFS) in 30 GEP-NEN patients candidate to therapy with mTOR inhibitor everolimus and with metachronous or progressive liver metastases. Only ASP > 12.9% (hazard ratio, HR), 3.33; p = 0.024) and prior RLT (HR, 0.35; p = 0.043) resulted statistically significant in multivariable Cox analysis. Moreover, when the ASP was above 12.9%, the median PFS was 6.7 months (95% CI: 2.1–11.4 months), whereas when it was below 12.9%, it was 14.4 (12.5–16.3) months (log-rank, p = 0.028).

Further studies evaluated the application of AI on the assessment of response to RLT on PET images: the assessment of response to RLT is still challenging, despite the fact that it seems to be one of the most successful treatment choices for metastatic, inoperable, well-differentiated GEP NETs. Particular attention has been paid to the evaluation of RFs capable of describing tumor heterogeneity, which is usually associated with a worse prognosis as a result of more aggressive biological behavior and treatment failure. In 2020, Weber et al. [46] aimed to assess changes in semiquantitative [^{68}Ga]Ga-DOTA-TOC PET/MRI parameters, including ADC, after different types of treatment including RLT. Although the study's sample size was too small to be statistically significant (only 9 patients underwent RLT), responding patients showed a significant decrease in lesion volume on ADC maps and a borderline significant decrease in entropy after RLT, even if non-statistically significant.

In two subsequent studies, Werner et al. [47] evaluated the prognostic value of baseline [^{68}Ga]Ga-DOTA-SSTa PET/CT RFs before RLT. RF entropy predicted both PFS and overall survival (OS) on a heterogenous cohort of 141 NET patients who were eligible for RLT (cut-off = 6.7, AUC = 0.71, p = 0.02), whereas conventional PET parameters did not show significant impacts. In a consecutive study [48] on a smaller, more homogeneous cohort of 31 pan-NET patients (G1/G2), the authors discovered a similar outcome: entropy was a predictor of overall survival (OS) at ROC analysis (cutoff = 6.7, AUC= 0.71, p = 0.02). Indeed, higher entropy indicated longer survival (OS = 2.5 years, 17/31, entropy > 6.7), whereas standard PET parameters were not.

In 2020, Önner et al. [49] evaluated tumor heterogeneity using the parameters skewness and kurtosis on pre- and post-treatment [^{68}Ga]Ga-DOTATATE PET/CT to assess therapy responses of 326 lesions (137 lesions responded partially or completely to the treatment, 189 lesions did not respond to treatment, remained stable or progressed) delineated from PET images of 22 GEP-NET patients treated with 2-6 therapy cycles of [^{177}Lu]Lu-DOTATATE. Lesions that did not respond to RLT had significantly higher skewness and kurtosis values than responder lesions (p < 0.001 and p = 0.004, respectively). However, ROC curves provided a moderate AUC value for skewness and a slightly lower value for kurtosis (0.619 and 0.518, respectively). Moreover, the authors did not compare the RF parameters with conventional PET parameters.

Preprints (www.preprints.org) | NOT PEER-REVIEWED | Posted: 9 June 2023 doi:10.20944/preprints202306.0677.v1

Subsequent studies have better analyzed this aspect, attempting to highlight the possible added value of radiomics parameters compared to conventional ones. In 2021, Ortega et al. [50] aimed to determine whether quantitative PET parameters (mean SUV_{max}, ratio to liver/spleen - T/L and T/S ratio -, SUV_{max}, SUV_{mean}, and heterogeneity parameters, such as CoV, kurtosis, and skewness) on baseline [^{68}Ga]Ga-DOTATATE PET/CT (bPET) and interim PET (iPET) performed prior to the second RLT cycle were predictive of therapy response and PFS on ninety-one NETs patients (71 responders and 20 non-responders). At bPET, higher mean SUV_{max} and mean SUV_{max} (Tumor/Liver ratio) were predictors of therapy response ($p = 0.018$ & 0.024, respectively); while higher SUV_{max} and SUV_{mean} and lower kurtosis were predictors of favorable response ($p = 0.025$, 0.0055 & 0.031, respectively) and correlated with longer PFS. From the multivariable analysis adjusted for age, primary site and Ki-67, mean SUV_{max} ($p = 0.019$), SUV_{max} T/L ($p = 0.018$), SUV_{max} T/S ($p = 0.041$), SUV_{mean} Liver ($p = 0.0052$) and skewness ($p = 0.048$) remained significant predictors of PFS. On the other hand, iPET parameters were not predictive of PFS, even if iPET was performed only for a subset of patients.

The same year, in a pilot report on two NET patients who experienced a discordant response to RLT (responder vs. non-responder) according to RECIST1.1, Liberini et al. [51] aimed to assess whether both tumor burden and radiomics parameters may have an added value over conventional parameters in predicting RLT response. They found that 28 RFs extracted from pre-therapy [^{68}Ga]Ga-DOTATOC PET/CT showed significant differences between the two patients in the Mann–Whitney test ($p < 0.05$) and the modifications of tumor burden parameter obtained from pre- and post-PRRT PET/CT correlated with RECIST1.1 response. Moreover, the authors concluded that seven second-order features with poor correlation with SUV_{max} and PET volume, identified by the Pearson correlation matrix, might have a role in defining inter-patient heterogeneity and in the prediction of therapy response.

The prognostic potential of tumor heterogeneity and tracer avidity in NET patients through a radiomics analysis of pre-RLT [^{68}Ga]Ga-DOTATATE PET/CT images has been also evaluated by Atkinson et al. [52] on 44 metastatic NET patients (carcinoid, pancreatic, thyroid, head and neck, catecholamine-secreting, and unknown primary NET). Measures of heterogeneity (higher kurtosis, higher entropy, and lower skewness) on coarse-texture scale CT and unfiltered PET images predicted shorter PFS (CT coarse kurtosis: $p = 0.05$, PET entropy: $p = 0.01$, PET skewness: $p = 0.03$) and shorter OS (CT coarse kurtosis: $p = 0.05$, PET entropy: $p = 0.01$, PET skewness $p = 0.02$). Multivariate analysis identified that CT-coarse kurtosis (HR = 2.57, 95% CI = 1.22–5.38, $p = 0.013$) independently predicted PFS, while PET-unfiltered skewness (HR = 9.05, 95% CI = 1.19–68.91, $p = 0.033$) independently predicted OS. Conventional PET parameters, such as SUV_{max} and SUV_{mean}, showed trends toward predicting outcomes but were not statistically significant.

Finally, in 2022, Laudicella et al. [53] retrospectively analyzed and compared the predictive value of conventional parameters, radiomics and Δradiomics parameters in 324 SSTR-2-positive lesions from 38 metastatic well-differentiated GEP-NET patients (9 G1, 27 G2, and 2 G3) who underwent restaging [^{68}Ga]Ga-DOTATOC PET/CT before complete RLT. The disease status for each lesion was determined by [^{68}Ga]Ga-DOTATOC PET/CT follow-up using the same scanner for each patient (progression vs. response in terms of stability, decrease, or disappearance). The k-fold approach was used to divide the data into training and validation sets and discriminant analysis was utilized to create the predictive model. Once again, SUV_{max} could not predict response to RLT ($p = 0.49$, AUC 0.523), while radiomics parameters proved to be superior to conventional quantitative parameters. From the reduction and selection process, HISTO_Skewness and HISTO_Kurtosis were able to predict RLT response with AUC, sensitivity, and specificity of 0.745, 80.6%, 67.2% and 0.72, 61.2%, 75.9%, respectively. In RLT-responsive lesions, the authors also observed a mean percentage reduction of the asymmetry (skewness) and a more evident increase in the "discrepancy of the considered histogram from the ordinary one" (Kurtosis) than non-responsive lesions. The most important characteristics and results of the above-mentioned studies are summarized in Table 3.

Preprints (www.preprints.org) | NOT PEER-REVIEWED | Posted: 9 June 2023 doi:10.20944/preprints202306.0677.v1

Table 3. Published articles concerning the implementation of radiomic and/or AI tools in the restaging of NEN patients.

Author	Year of Publication	Study Design	NET Type	Number of patients	Source of data	Software	AI application	Validation	Findings
Nogueira et al. [69]	2017	retrospective	NENs	34	[^{18}F]FDG and [^{68}Ga]DOTA-peptides PET/CT	NA	Yes	No	LVQNN assured classification accuracies of 100%, 100%, 96.3%, and 100% regarding the 4 response-to-treatment classes (negative, neutral, positive incomplete and positive complete)
Wetz et al. [70]	2016	retrospective	GEP-NENs	20	[^{111}In]DTPA-octreotide scintigraphy	ROVER version 2.1.20 (ABX, Radeberg, Germany)	No	No	a higher ASP level was associated with poorer response to RLT
Wetz et al. [71]	2020	retrospective	GEP-NENs	30	[^{111}In]DTPA-octreotide scintigraphy	ROVER version 2.1.20 (ABX, Radeberg, Germany)	No	No	ASP > 12.9% ($p = 0.024$) resulted statistically significant in multivariable Cox analysis to predicte response to everolimus
Weber et al. [72]	2020	retrospective	All NENs	18	[^{68}Ga]DOTA-peptides PET/MRI	LIFEx	No	No	PRRT-responding patients (9 pts) showed a significant decrease in lesion volume on ADC maps and a borderline significant decrease in entropy after RLT, even if non-statistically significant
Werner et al. [73	2017	retrospective	All NENs (108 GEP-NET)	141	[^{68}Ga]DOTA-peptides PET/CT	Interview Fusion Workstation (Mediso Medical Imaging Systems Ltd., Budapest, Hungary)	No	No	RF entropy predicted both PFS and overall survival (OS) (cut-off = 6.7, AUC = 0.71, $p = 0.02$), without significant results for conventional PET parameters
Werner et al. [74]	2019	retrospective	Pan-NET	31	[^{68}Ga]DOTA-peptides PET/CT	Interview Fusion Workstation (Mediso Medical Imaging Systems Ltd., Budapest, Hungary)	No	No	entropy was predictive for OS (cutoff = 6.7, AUC= 0.71, p= 0.02); indeed, an increased entropy predicted longer survival (entropy > 6.7, OS = 2.5 years, 17/31), while conventional PET parameters failed to predict patient outcome
Önner et al. [75]	2020	retrospective	GEP-NET	22	[^{68}Ga]DOTA-peptides PET/CT	LIFEx	No	No	The skewness and kurtosis values of the lesions which did not respond to RLT were significantly higher than those with a response ($p < 0.001$ and $p = 0.004$, respectively).

 doi:10.20944/preprints202306.0677.v1

Ortega et al. [52]	2021	retrospective	All NENs	91	[^{68}Ga]DOTA-peptides PET/CT	nuclear medicine PACS system with fusion software (Mirada Medical)	No	No	At baseline-PET, from the multivariable analysis, mean SUV_{max} ($p = 0.019$), SUV_{max} T/L ($p = 0.018$), SUV_{max} T/S ($p = 0.041$), SUV_{mean} Liver ($p = 0.0052$) and skewness ($p = 0.048$) remained significant predictors of PFS after RLT. On the other hand, interim-PET parameters were not predictive of PFS.
Liberini et al. [76]	2021	retrospective	GEP-NEC	2	[^{68}Ga]DOTA-peptides PET/CT	LIFEx	No	No	28 RFs extracted from pre-therapy PET/CT showed significant differences between the two patients in the Mann–Whitney test ($p < 0.05$) and the modifications of tumor burden parameter obtained from pre- and post-PRRT PET/CT correlated with RECIST1.1 response
Atkinson et al. [77]	2021	retrospective	All NENs	44	[^{68}Ga]DOTA-peptides PET/CT	TexRAD research software (TexRAD, part of Feedback Medical Ltd, www.fbkmed.com, Cambridge, UK)	No	No	Multivariate analysis identified that CT-coarse kurtosis (HR = 2.57, 95% CI = 1.22–5.38, $p = 0.013$) independently predicted PFS, while PET-unfiltered skewness (HR = 9.05, 95% CI = 1.19–68.91, $p = 0.033$) independently predicted OS
Laudicella et al. [78]	2022	retrospective	GEP-NET	38	[^{68}Ga]DOTA-peptides PET/CT	LIFEx	Yes	Yes	SUV_{max} could not predict response to RLT ($p = 0.49$, AUC 0.523), while HISTO_Skewness and HISTO_Kurtosis were able to predict RLT response with AUC, sensitivity, and specificity of 0.745, 80.6%, 67.2% and 0.72, 61.2%, 75.9%, respectively

Preprints (www.preprints.org) | NOT PEER-REVIEWED | Posted: 9 June 2023 doi:10.20944/preprints202306.0677.v1

4. Technical Applications

Although the scientific interest in AI applied to PET imaging is rapidly growing, the methodological approach needs to be validated and standardized prior to its potential use in clinical settings [22,24,54]. The term robustness is often used to indicate the repeatability and reproducibility of the RFs evaluated with different acquisition and processing conditions. In the literature, there are several studies for the evaluation of RFs robustness in [^{18}F]FDG PET/TC imaging, while only a few have yet been published on [^{68}Ga]Ga-DOTA-peptides PET/CT imaging.

In 2016, Bailly et al. [55] aimed to evaluate the robustness of RFs extracted from [^{68}Ga]Ga-DOTANOC PET images of twenty-six GEP-NET patients, as a function of acquisition and reconstruction parameters within the context of multi-centric trials. All datasets were reconstructed using four different algorithms, three different matrix size and, for each reconstruction algorithm, three different numbers of iterations. They found that only Entropy, Energy, RP, and ZP resulted in adequate robustness with respect to the number of iterations, the post-filtering level, the noise in input data, and the reconstruction algorithm used. In contrast, Correlation and LZLGE were found to be very sensitive to the aforementioned parameters. Moreover, the voxel size used to reconstruct PET images severely impacted the RF Correlation, Energy, Contrast, and Dissimilarity, LGRE, ZLNU, LGZE, and LZLGE RFs. Only Entropy and RP had a variability that was comparable to SUV_{mean}.

Compared to [^{18}F]FDG, [^{68}Ga]Ga-DOTA-peptides have a significantly different physiological distribution and showed more inter- and intra-patient heterogeneity for physiological and pathological uptake, requiring the use of different methods of segmentation and different discretization settings. On this premise, in 2021, Liberini et al. [56] sought to identify robust RFs extracted from [^{68}Ga]Ga-DOTATOC PET images of forty-nine NET patients, as a result of different segmentation (manual contouring applying three different fixed SUV_{max} thresholds of 20, 30, and 40% respectively, versus a semi-automated edge-based segmentation algorithm - SAEB) and grey-level intensity discretization (an absolute one, namely AR60 = SUV from 0 to 60, and a relative one, namely RR = min-max of VOI's SUV) methods. Of 51 RFs extracted with the open-source IBSI-compliant Lifex software [57], 64.7% (7/10 conventional, 3/6 histogram, 2/4 shape, and 21/31 textual) showed high robustness in terms of consistency (intra-class correlation coefficients – ICC > 0.9) and agreement (low median coefficient of variance, COV_L) between different operators, improved by applying SUV_{max} threshold of 40% (86.5%). Furthermore, the dice similarity coefficient (DSC) mean value was 0.75 ± 0.11 (0.45-0.92) between SAEB and operators and 0.78 ± 0.09 (0.36-0.97), among the four manual segmentations, suggesting that SAEB segmentation could be an optimal alternative to manual segmentation, even if further validations are needed. Finally, the use of the absolute intensity scaling factor (AR60) achieved greater robustness of RF to segmentation than the relative intensity scaling factor (RR).

Although RF robustness is high using the manual contouring with the 40% fixed SUV_{max} thresholds, this approach is time-consuming; moreover, it may lead to the loss of important biological information and a reduction of analyzable lesions with textural characteristics due to the low number of voxels not sufficient to perform a radiomics analysis. For that reason, various semi-automatic and automatic segmentation methods were evaluated for both single lesion and total tumor burden segmentation [50,58–65]. Two different studies have recently developed an AI-based automatic lesion segmentation technique in NET patients. In 2021, Wehrend et al. [66] developed an automated method to identify liver lesions by [^{68}Ga]Ga-DOTATE PET/CT using a 2D fully convolutional, U-Net-like neural network, trained by minimizing a linear combination of binary cross-entropy loss and dice loss with a stochastic gradient descent algorithm for 100,000 iterations. The model was performed on 125 patients (57 with PET-positive liver lesions and 68 without) randomly divided into 75 patients for the training set (36 abnormal, 39 normal), 25 for the validation set (11 abnormal, 14 normal), and 25 for the test set (11 abnormal, 14 normal). In this study, manual liver segmentation and semi-automated annotation of lesions were used as the ground truth: the authors used a modified PERCIST threshold for liver lesions identification and a commercially available gradient edge detection tool (PET Edge plus; MIM 7.0.3 software) to define lesion boundaries. A total of 233 lesions

Preprints (www.preprints.org) | NOT PEER-REVIEWED | Posted: 9 June 2023 doi:10.20944/preprints202306.0677.v1

were annotated with each abnormal study containing a mean of 4 ± 2.75 lesions. To reduce the effects of noisy predictions, filters based on pixel area were applied to remove values below a certain threshold: the highest mean positive predictive value (PPV) of 0.94 ± 0.01 and the highest mean F1 score of 0.79 ± 0.01 were produced with a 20-pixel filter, while the highest mean area under the precision–recall curve (PR-AUC) of 0.73 ± 0.03 was produced with a 15-pixel filter. The most common sources of error reported for false-positive lesions were lesions close to the edge of a true lesion, with a score above the PERCIST limit, but disagreed with the annotated gold standard (6/12; 50%); while for false-negative lesions were lesions with low uptake.

In 2022, Carlsen et al. [67] investigated the performance of an AI network, with deep learning U-Net architecture, for tumor segmentation of [^{64}Cu]Cu-DOTATATE PET/CT images of GEP-NEN and lung-NEN patients (117 in training, 41 in testing, and 10 patients without signs of NEN included as negative controls). Ground truth segmentations were obtained by a standardized semiautomatic method for tumor segmentation. Although the ensemble model obtained rather high values of lesion-wise dice index, pixel-wise dice index, precision, and sensitivity (0.85, 0.8, 0.79, and 0.87, respectively), some degree of manual adjustment was required in 85% (35/41) patients to consider the performance of the model as acceptable. Nevertheless, the AI model appeared to be faster than the ground truth (semi-automatic) method, reducing manual adjustment time to 5 minutes (vs. 17 minutes, $p < 0.01$). Among the limitations of the evaluated AI model, the authors reported: - the need to manually remove false-positive segmentations (such as adrenal gland or bladder) and/or to add lesions not included in the segmentation; - the elimination of all lesions smaller than 0.1 mL (lesions < 9 voxels) to reduce segmentation of noise; - a non-homogeneous training and testing cohort due to a higher frequency of primary small bowel and pancreatic tumors and grade 2 patients (although the Ki-67 index was not significantly different between patients).

Another interesting application of AI is the automatic segmentation of healthy organs and tumor lesions for patient-specific dosimetry in radiopharmaceutical treatment (RPT) for the development and validation of individualized protocols to provide personalized therapy. In 2021, Khan et al. [68] developed a convolution neural network (CNN) for automated kidney segmentation that accurately aligns CT segmented volume of interest (VOI) to the kidneys in SPECT images, trained with SPECT/CT images performed over the abdominal area of 137 patients treated with RLT. The Bland-Altman analysis demonstrated higher accuracy for the CNN segmentation compared to the manual-segmented kidneys without VOI adjustment, with the benefit of reduced operating time. Similarly, in 2022, Dewaraja et al. [69] aimed to construct and test an integrated voxel-level pipeline (CNNs) that automates key components (organ segmentation, registration, dose-rate estimation, and curve fitting) on CT of SPECT/CT of the RPT dosimetry process and then use it to report patient-specific dosimetry in 20 patients candidate to RLT. Indeed, the organs on CT of SPECT/CT are automatically segmented using CNNs; then, the VOI propagation to other time-point is achieved by local contour intensity-based SPECT-SPECT alignment. Dose-rate estimation is performed by explicit Monte Carlo (MC) using the fast, Dose-Planning Method code, and the best function for dose-rate fitting is automatically chosen for each voxel. CNN-defined kidneys resulted in high Dice index values (0.91-0.94) and only small differences (2-5%) in mean dose when compared with manual segmentation. For a typical patient, the time for the entire process was ~ 25 minutes on a desktop computer, including the time for CNN organ segmentation, co-registration, MC dosimetry and voxel curve fitting.

Finally, Ding et al. [70], based on the dynamic acquisitions carried out separately on two different days, examined the efficacy of using a machine learning-based algorithm for rapid dual-tracer ([^{18}F]FDG and [^{68}Ga]Ga-DOTATATE) simulated dynamic PET acquisition protocol in a single imaging session with NET imaging data of twelve NET patients. Authors developed a recurrent extreme gradient boosting (rXGBoost) machine learning algorithm to separate the mixed [^{18}F]FDG and [^{68}Ga]Ga-DOTATATE time activity curves (TACs) for the region of interest (ROI) based quantification with tracer kinetic modeling. The results of this preliminary analysis were quite encouraging: - the correlation coefficient of the proposed method was higher than that of the parallel multi-tracer compartment model (PMCM); - the algorithm can effectively reduce the total scanning

Preprints (www.preprints.org) | NOT PEER-REVIEWED | Posted: 9 June 2023 doi:10.20944/preprints202306.0677.v1

time by shortening the stagger time of the two tracers; - high accuracy was still maintained when the simulated delay between the two tracers' injection was only 5 minutes.

5. Discussion

This review highlights the state of the art of AI in the scenario of NETs in nuclear medicine, revealing how several reasons make this field still in its preliminary state.

NENs are relatively rare and extremely heterogeneous tumors, which makes it difficult to have a large and adequately homogeneous sample of patients.

Imaging analysis procedures such as tumor segmentation methods, grey-level intensity discretization and image reconstruction algorithms can affect the robustness, repeatability and reproducibility of radiomics variables and their results: while the more widespread use of [^{18}F]FDG PET/CT in clinical practice, as a metabolic tracer, has led to a significantly larger evaluation of the robustness of radiomics studies, considerably fewer studies have evaluated this aspect in [^{68}Ga]DOTA-peptides PET/CT imaging.

In clinical studies, authors examined the potential of radiomics for several key objectives in the management of NENs patients: prediction of tumor grade, prognostic assessment, and prediction of response to RLT. Despite the attractive results reported above, there is still considerable work required to apply the results of this research in clinical practice: a prospective, sufficiently large and homogeneous study sample is hardly available due to the rarity of NENs; furthermore, NENs patients barely perform dual-imaging evaluation with [^{18}F]FDG and [^{68}Ga]Ga-DOTA-peptides PET to evaluate the "NETPET score", and the inherent heterogeneity of these tumors makes a standardized approach in the methodology applied to PET imaging difficult compared to other tumors (high variability of uptake for both [^{18}F]FDG and [^{68}Ga]Ga-DOTA-peptides PET imaging compared to other tumors). [^{68}Ga]Ga-DOTA-peptides PET imaging is considered the state of the art to quantify SST receptors in vivo, while [^{18}F]FDG is used to metabolically characterize more aggressive and higher grade NET lesions; consequently, it may be difficult to identify and segment the most aggressive lesions on only [^{68}Ga]Ga-DOTA-peptides images, especially for lesions with low SST receptor expression (low SUV_{max} values).. Moreover, the majority of the described studies are exploratory with univariable analyses, lacking external validation. Also, many studies were conducted before the drafting of the IBSI, which aims to provide image biomarker nomenclature and definitions, and of the new European Association of Nuclear Medicine (EANM) and the Society of Nuclear Medicine and Molecular Imaging (SNMMI) guidelines for pertinent study design, quality control, data collection, the effects of acquisition and reconstruction, detection and segmentation, standardization, and feature implementation, as well as adequate modeling schemes, model assessment, and interpretation [17,22,24,71].

Nonetheless, some encouraging results obtained through the above-mentioned articles suggest that a significant role in 'non-invasive' patient management in the clinical practice and in the clinical decision support system (CDSS) could be played by some RFs in the future, such as first-order statistics, metabolic tumor burden (MTB) from [^{18}F]FDG PET/CT images, somatostatin receptor tumor burden (SRTB) from [^{68}Ga]Ga-DOTA-peptides PET/CT images and GLRLM features. Moreover, the publication of negative results in the radiomics field is also very relevant to understand the directions for meaningful future research. Based on the presented results, technical and clinical studies that used radiomics for the prediction of response or long-term outcome seem to be more relevant endpoints compared with studies focused on the identification of tumor grade, since these latter presumably require even more large and homogeneous samples and the availability of several data (histopathological, genetic, radiological, and nuclear medical).

6. Conclusions

Clinically and physiologically, NENs range from quite indolent to extremely aggressive neoplasms. Both the staging and the histological grading affect their prognosis and course of treatment since less differentiated NENs are more likely to be aggressive and have a poor prognosis

 doi:10.20944/preprints202306.0677.v1

than well-differentiated tumors. The scientific community is giving increasing attention to AI techniques due to a variety of potential applications in the NEN field, ranging from the technical aspects of image reconstruction and segmentation to clinical and therapeutic aspects. However, a large workload and numerous validation and rigorous studies following new radiomics and AI guidelines are still required to implement most of these strategies in clinical practice.

7. Patents

Author Contributions: Substantial contributions to the conception or design of the work: VL; Literature search: RL, EG and SG; Article selection: MB, RL, EG, SG and VL; Drafting of the manuscript: MB and VL; Critical revision of the manuscript for important intellectual content: all authors. All authors have read and agreed to the published version of the manuscript.

Funding: This research received no external funding.

Institutional Review Board Statement: Not applicable.

Informed Consent Statement: Not applicable.

Data Availability Statement: Not applicable.

Conflicts of Interest: The authors declare no conflict of interest.

References

1. Yao, J.C.; Hassan, M.; Phan, A.; Dagohoy, C.; Leary, C.; Mares, J.E.; Abdalla, E.K.; Fleming, J.B.; Vauthey, J.N.; Rashid, A.; et al. One hundred years after "carcinoid": Epidemiology of and prognostic factors for neuroendocrine tumors in 35,825 cases in the United States. *J. Clin. Oncol.* **2008**, *26*, 3063–3072, doi:10.1200/JCO.2007.15.4377.
2. Rindi, G.; Mete, O.; Uccella, S.; Basturk, O.; La Rosa, S.; Brosens, L.A.A.; Ezzat, S.; de Herder, W.W.; Klimstra, D.S.; Papotti, M.; et al. Overview of the 2022 WHO Classification of Neuroendocrine Neoplasms. *Endocr. Pathol.* 2022, *33*, 115–154.
3. Mete, O.; Wenig, B.M. Update from the 5th Edition of the World Health Organization Classification of Head and Neck Tumors: Overview of the 2022 WHO Classification of Head and Neck Neuroendocrine Neoplasms. *Head Neck Pathol.* **2022**, *16*, 123–142, doi:10.1007/s12105-022-01435-8.
4. Bogaards, M.; May, A.M.; Hassan, F.A.; Valk, G.D.; van Leeuwaarde, R.S. Lifestyle factors and development and natural course of gastroenteropancreatic neuroendocrine tumors (GEP-NETs): a review of the literature. *Neuroendocrinology* **2022**, doi:10.1159/000527741.
5. Choi, J.H.; Paik, W.H. Risk Stratification of Pancreatic Neuroendocrine Neoplasms Based on Clinical, Pathological, and Molecular Characteristics. *J. Clin. Med.* 2022, *11*.
6. Papotti, M.; Bongiovanni, M.; Volante, M.; Allìa, E.; Landolfi, S.; Helboe, L.; Schindler, M.; Cole, S.; Bussolati, G. Expression of somatostatin receptor types 1-5 in 81 cases of gastrointestinal and pancreatic endocrine tumors: A correlative immunohistochemical and reverse-transcriptase polymerase chain reaction analysis. *Virchows Arch.* **2002**, *440*, 461–475, doi:10.1007/s00428-002-0609-x.
7. Geijer, H.; Breimer, L.H. Somatostatin receptor PET/CT in neuroendocrine tumours: Update on systematic review and meta-analysis. *Eur. J. Nucl. Med. Mol. Imaging* 2013, *40*, 1770–1780.
8. Pauwels, E.; Cleeren, F.; Bormans, G.; Deroose, C.M. Somatostatin receptor PET ligands - the next generation for clinical practice. *Am. J. Nucl. Med. Mol. Imaging* **2018**, *8*, 311–331.
9. Sundin, A.; Arnold, R.; Baudin, E.; Cwikla, J.B.; Eriksson, B.; Fanti, S.; Fazio, N.; Giammarile, F.; Hicks, R.J.; Kjaer, A.; et al. ENETS Consensus Guidelines for the Standards of Care in Neuroendocrine Tumors: Radiological, Nuclear Medicine and Hybrid Imaging. In Proceedings of the Neuroendocrinology; S. Karger AG, 2017; Vol. 105, pp. 212–244.
10. Bozkurt, M.F.; Virgolini, I.; Balogova, S.; Beheshti, M.; Rubello, D.; Decristoforo, C.; Ambrosini, V.; Kjaer, A.; Delgado-Bolton, R.; Kunikowska, J.; et al. Guideline for PET/CT imaging of neuroendocrine neoplasms with 68Ga-DOTA-conjugated somatostatin receptor targeting peptides and 18F–DOPA. *Eur. J. Nucl. Med. Mol. Imaging* **2017**, *44*, 1588–1601, doi:10.1007/s00259-017-3728-y.
11. Zaknun, J.J.; Bodei, L.; Mueller-Brand, J.; Pavel, M.E.; Baum, R.P.; Hörsch, D.; O'Dorisio, M.S.; O'Dorisiol, T.M.; Howe, J.R.; Cremonesi, M.; et al. The joint IAEA, EANM, and SNMMI practical guidance on peptide

receptor radionuclide therapy (PRRNT) in neuroendocrine tumours. *Eur. J. Nucl. Med. Mol. Imaging* 2013, *40*, 800–816.

12. Virgolini, I.; Ambrosini, V.; Bomanji, J.B.; Baum, R.P.; Fanti, S.; Gabriel, M.; Papathanasiou, N.D.; Pepe, G.; Oyen, W.; De Cristoforo, C.; et al. Procedure guidelines for PET/CT tumour imaging with 68Ga-DOTA-conjugated peptides: 68Ga-DOTA-TOC, 68Ga-DOTA-NOC, 68Ga-DOTA-TATE. *Eur. J. Nucl. Med. Mol. Imaging* **2010**, *37*, 2004–2010, doi:10.1007/s00259-010-1512-3.
13. Panagiotidis, E.; Alshammari, A.; Michopoulou, S.; Skoura, E.; Naik, K.; Maragkoudakis, E.; Mohmaduvesh, M.; Al-Harbi, M.; Belda, M.; Caplin, M.E.; et al. Comparison of the impact of 68Ga-DOTATATE and 18F-FDG PET/CT on clinical management in patients with Neuroendocrine tumors. *J. Nucl. Med.* **2017**, *58*, 91–96, doi:10.2967/jnumed.116.178095.
14. Chan, D.L.H.; Pavlakis, N.; Schembri, G.P.; Bernard, E.J.; Hsiao, E.; Hayes, A.; Barnes, T.; Diakos, C.; Khasraw, M.; Samra, J.; et al. Dual somatostatin receptor/FDG PET/CT imaging in metastatic neuroendocrine tumours: Proposal for a novel grading scheme with prognostic significance. *Theranostics* **2017**, *7*, 1149–1158, doi:10.7150/thno.18068.
15. Hatt, M.; Tixier, F.; Pierce, L.; Kinahan, P.E.; Le Rest, C.C.; Visvikis, D. Characterization of PET/CT images using texture analysis: the past, the present… any future? *Eur. J. Nucl. Med. Mol. Imaging* 2017, *44*, 151–165.
16. Ha, S.; Choi, H.; Paeng, J.C.; Cheon, G.J. Radiomics in Oncological PET/CT: a Methodological Overview. *Nucl. Med. Mol. Imaging (2010).* 2019, *53*, 14–29.
17. Lambin, P.; Rios-Velazquez, E.; Leijenaar, R.; Carvalho, S.; Van Stiphout, R.G.P.M.; Granton, P.; Zegers, C.M.L.; Gillies, R.; Boellard, R.; Dekker, A.; et al. Radiomics: Extracting more information from medical images using advanced feature analysis. *Eur. J. Cancer* **2012**, *48*, 441–446, doi:10.1016/j.ejca.2011.11.036.
18. Gillies, R.J.; Kinahan, P.E.; Hricak, H. Radiomics: Images are more than pictures, they are data. *Radiology* **2016**, *278*, 563–577, doi:10.1148/radiol.2015151169.
19. Sanduleanu, S.; Woodruff, H.C.; de Jong, E.E.C.; van Timmeren, J.E.; Jochems, A.; Dubois, L.; Lambin, P. Tracking tumor biology with radiomics: A systematic review utilizing a radiomics quality score. *Radiother. Oncol.* 2018, *127*, 349–360.
20. Zwanenburg, A.; Vallières, M.; Abdalah, M.A.; Aerts, H.J.W.L.; Andrearczyk, V.; Apte, A.; Ashrafinia, S.; Bakas, S.; Beukinga, R.J.; Boellaard, R.; et al. The image biomarker standardization initiative: Standardized quantitative radiomics for high-throughput image-based phenotyping. *Radiology* **2020**, *295*, 328–338, doi:10.1148/radiol.2020191145.
21. Mayerhoefer, M.E.; Materka, A.; Langs, G.; Häggström, I.; Szczypiński, P.; Gibbs, P.; Cook, G. Introduction to Radiomics. *J. Nucl. Med.* 2020, *61*, 488–495.
22. Zwanenburg, A.; Leger, S.; Vallières, M.; Löck, S. Image biomarker standardisation initiative. **2016**.
23. Zwanenburg, A.; Vallières, M.; Abdalah, M.A.; Aerts, H.J.W.L.; Andrearczyk, V.; Apte, A.; Ashrafinia, S.; Bakas, S.; Beukinga, R.J.; Boellaard, R.; et al. The image biomarker standardization initiative: Standardized quantitative radiomics for high-throughput image-based phenotyping. *Radiology* **2020**, *295*, 328–338, doi:10.1148/radiol.2020191145.
24. Hatt, M.; Krizsan, A.K.; Rahmim, A.; Bradshaw, T.J.; Costa, P.F.; Forgacs, A.; Seifert, R.; Zwanenburg, A.; El Naqa, I.; Kinahan, P.E.; et al. Joint EANM/SNMMI guideline on radiomics in nuclear medicine. *Eur. J. Nucl. Med. Mol. Imaging* **2022**, 1–24, doi:10.1007/s00259-022-06001-6.
25. Avanzo, M.; Porzio, M.; Lorenzon, L.; Milan, L.; Sghedoni, R.; Russo, G.; Massafra, R.; Fanizzi, A.; Barucci, A.; Ardu, V.; et al. Artificial intelligence applications in medical imaging: A review of the medical physics research in Italy. *Phys. Medica* **2021**, *83*, 221–241, doi:10.1016/j.ejmp.2021.04.010.
26. Yousefirizi, F.; Pierre Decazes; Amyar, A.; Ruan, S.; Saboury, B.; Rahmim, A. AI-Based Detection, Classification and Prediction/Prognosis in Medical Imaging:: Towards Radiophenomics. *PET Clin.* 2022, *17*, 183–212.
27. Hasani, N.; Morris, M.A.; Rhamim, A.; Summers, R.M.; Jones, E.; Siegel, E.; Saboury, B. Trustworthy Artificial Intelligence in Medical Imaging. *PET Clin.* 2022, *17*, 1–12.
28. Goldenberg, S.L.; Nir, G.; Salcudean, S.E. A new era: artificial intelligence and machine learning in prostate cancer. *Nat. Rev. Urol.* 2019, *16*, 391–403.
29. Panayides, A.S.; Amini, A.; Filipovic, N.D.; Sharma, A.; Tsaftaris, S.A.; Young, A.; Foran, D.; Do, N.; Golemati, S.; Kurc, T.; et al. AI in Medical Imaging Informatics: Current Challenges and Future Directions. *IEEE J. Biomed. Heal. Informatics* 2020, *24*, 1837–1857.

30. Liberati, A.; Altman, D.G.; Tetzlaff, J.; Mulrow, C.; Gøtzsche, P.C.; Ioannidis, J.P.A.; Clarke, M.; Devereaux, P.J.; Kleijnen, J.; Moher, D. The PRISMA statement for reporting systematic reviews and meta-analyses of studies that evaluate health care interventions: explanation and elaboration. In Proceedings of the Journal of clinical epidemiology; J Clin Epidemiol, 2009; Vol. 62, pp. e1–e34.
31. Oberg, K.; Krenning, E.; Sundin, A.; Bodei, L.; Kidd, M.; Tesselaar, M.; Ambrosini, V.; Baum, R.P.; Kulke, M.; Pavel, M.; et al. A delphic consensus assessment: Imaging and biomarkers in gastroenteropancreatic neuroendocrine tumor disease management. *Endocr. Connect.* **2016**, *5*, 174–187, doi:10.1530/EC-16-0043.
32. Giesel, F.L.; Schneider, F.; Kratochwil, C.; Rath, D.; Moltz, J.; Holland-Letz, T.; Kauczor, H.U.; Schwartz, L.H.; Haberkorn, U.; Flechsig, P. Correlation between SUVmax and CT radiomic analysis using lymph node density in PET/CT-based lymph node staging. *J. Nucl. Med.* **2017**, *58*, 282–287, doi:10.2967/jnumed.116.179648.
33. Weber, M.; Kessler, L.; Schaarschmidt, B.; Fendler, W.P.; Lahner, H.; Antoch, G.; Umutlu, L.; Herrmann, K.; Rischpler, C. Textural analysis of hybrid DOTATOC-PET/MRI and its association with histological grading in patients with liver metastases from neuroendocrine tumors. *Nucl. Med. Commun.* **2020**, *41*, 363–369, doi:10.1097/MNM.0000000000001150.
34. Thuillier, P.; Liberini, V.; Rampado, O.; Gallio, E.; De Santi, B.; Ceci, F.; Metovic, J.; Papotti, M.; Volante, M.; Molinari, F.; et al. Diagnostic value of conventional pet parameters and radiomic features extracted from 18f-fdg-pet/ct for histologic subtype classification and characterization of lung neuroendocrine neoplasms. *Biomedicines* **2021**, *9*, 1–14, doi:10.3390/biomedicines9030281.
35. Fonti, R.; Panico, M.; Pellegrino, S.; Pulcrano, A.; Vastarella, L.A.; Torbati, A.H.M.; Giuliano, M.; Palmieri, G.; De Placido, S.; Del Vecchio, S. Heterogeneity of SSTR2 Expression Assessed by 68Ga-DOTATOC PET/CT Using Coefficient of Variation in Patients with Neuroendocrine Tumors. *J. Nucl. Med.* **2022**, *63*, 1509–1514, doi:10.2967/jnumed.121.262928.
36. Mapelli, P.; Partelli, S.; Salgarello, M.; Doraku, J.; Pasetto, S.; Rancoita, P.M.V.; Muffatti, F.; Bettinardi, V.; Presotto, L.; Andreasi, V.; et al. Dual tracer 68Ga-DOTATOC and 18F-FDG PET/computed tomography radiomics in pancreatic neuroendocrine neoplasms: An endearing tool for preoperative risk assessment. *Nucl. Med. Commun.* **2020**, *41*, 896–905, doi:10.1097/MNM.0000000000001236.
37. Mapelli, P.; Bezzi, C.; Palumbo, D.; Canevari, C.; Ghezzo, S.; Samanes Gajate, A.M.; Catalfamo, B.; Messina, A.; Presotto, L.; Guarnaccia, A.; et al. 68Ga-DOTATOC PET/MR imaging and radiomic parameters in predicting histopathological prognostic factors in patients with pancreatic neuroendocrine well-differentiated tumours. *Eur. J. Nucl. Med. Mol. Imaging* **2022**, *49*, 2352–2363, doi:10.1007/s00259-022-05677-0.
38. Bevilacqua, A.; Calabrò, D.; Malavasi, S.; Ricci, C.; Casadei, R.; Campana, D.; Baiocco, S.; Fanti, S.; Ambrosini, V. A [68ga]ga-dotanoc pet/ct radiomic model for non-invasive prediction of tumour grade in pancreatic neuroendocrine tumours. *Diagnostics* **2021**, *11*, doi:10.3390/diagnostics11050870.
39. Noortman, W.A.; Vriens, D.; de Geus-Oei, L.F.; Slump, C.H.; Aarntzen, E.H.; van Berkel, A.; Timmers, H.J.L.M.; van Velden, F.H.P. [18F]FDG-PET/CT radiomics for the identification of genetic clusters in pheochromocytomas and paragangliomas. *Eur. Radiol.* **2022**, *32*, 7227–7236, doi:10.1007/s00330-022-09034-5.
40. Schork, N.J. Personalized medicine: Time for one-person trials. *Nature* 2015, *520*, 609–611.
41. Cook, G.J.R.; Azad, G.; Owczarczyk, K.; Siddique, M.; Goh, V. Challenges and Promises of PET Radiomics. *Int. J. Radiat. Oncol. Biol. Phys.* **2018**, *102*, 1083–1089, doi:10.1016/j.ijrobp.2017.12.268.
42. Liberini, V.; Huellner, M.W.; Grimaldi, S.; Finessi, M.; Thuillier, P.; Muni, A.; Pellerito, R.E.; Papotti, M.G.; Piovesan, A.; Arvat, E.; et al. The Challenge of Evaluating Response to Peptide Receptor Radionuclide Therapy in Gastroenteropancreatic Neuroendocrine Tumors: The Present and the Future. *Diagnostics* **2020**, *10*, 1083, doi:10.3390/diagnostics10121083.
43. Nogueira, M.A.; Abreu, P.H.; Martins, P.; Machado, P.; Duarte, H.; Santos, J. An artificial neural networks approach for assessment treatment response in oncological patients using PET/CT images. *BMC Med. Imaging* **2017**, *17*, doi:10.1186/s12880-017-0181-0.
44. Wetz, C.; Apostolova, I.; Steffen, I.G.; Hofheinz, F.; Furth, C.; Kupitz, D.; Ruf, J.; Venerito, M.; Klose, S.; Amthauer, H. Predictive Value of Asphericity in Pretherapeutic [111In]DTPA-Octreotide SPECT/CT for Response to Peptide Receptor Radionuclide Therapy with [177Lu]DOTATATE. *Mol. Imaging Biol.* **2017**, *19*, 437–445, doi:10.1007/s11307-016-1018-x.

45. Wetz, C.; Rogasch, J.; Genseke, P.; Schatka, I.; Furth, C.; Kreissl, M.; Jann, H.; Venerito, M.; Amthauer, H. Asphericity of somatostatin receptor expression in neuroendocrine tumors: an innovative predictor of outcome in everolimus treatment? *Diagnostics* **2020**, *10*, doi:10.3390/diagnostics10090732.
46. Weber, M.; Kessler, L.; Schaarschmidt, B.; Fendler, W.P.; Lahner, H.; Antoch, G.; Umutlu, L.; Herrmann, K.; Rischpler, C. Treatment-related changes in neuroendocrine tumors as assessed by textural features derived from 68Ga-DOTATOC PET/MRI with simultaneous acquisition of apparent diffusion coefficient. *BMC Cancer* **2020**, *20*, doi:10.1186/s12885-020-06836-y.
47. Werner, R.A.; Lapa, C.; Ilhan, H.; Higuchi, T.; Buck, A.K.; Lehner, S.; Bartenstein, P.; Bengel, F.; Schatka, I.; Muegge, D.O.; et al. Survival prediction in patients undergoing radionuclide therapy based on intratumoral somatostatin-receptor heterogeneity. *Oncotarget* **2017**, *8*, 7039–7049, doi:10.18632/oncotarget.12402.
48. Werner, R.A.; Ilhan, H.; Lehner, S.; Papp, L.; Zsótér, N.; Schatka, I.; Muegge, D.O.; Javadi, M.S.; Higuchi, T.; Buck, A.K.; et al. Pre-therapy Somatostatin Receptor-Based Heterogeneity Predicts Overall Survival in Pancreatic Neuroendocrine Tumor Patients Undergoing Peptide Receptor Radionuclide Therapy. *Mol. Imaging Biol.* **2019**, *21*, 582–590, doi:10.1007/s11307-018-1252-5.
49. Önner, H.; Abdülrezzak, Ü.; Tutuş, A. Could the skewness and kurtosis texture parameters of lesions obtained from pretreatment Ga-68 DOTA-TATE PET/CT images predict receptor radionuclide therapy response in patients with gastroenteropancreatic neuroendocrine tumors? *Nucl. Med. Commun.* **2020**, *41*, 1034–1039, doi:10.1097/MNM.0000000000001231.
50. Ortega, C.; Wong, R.K.S.; Schaefferkoetter, J.; Veit-Haibach, P.; Myrehaug, S.; Juergens, R.; Laidley, D.; Anconina, R.; Liu, A.; Metser, U. Quantitative 68Ga-Dotatate PET/CT parameters for the prediction of therapy response in patients with progressive metastatic neuroendocrine tumors treated with 177Lu-Dotatate. *J. Nucl. Med.* **2021**, *62*, doi:10.2967/jnumed.120.256727.
51. Liberini, V.; Rampado, O.; Gallio, E.; De Santi, B.; Ceci, F.; Dionisi, B.; Thuillier, P.; Ciuffreda, L.; Piovesan, A.; Fioroni, F.; et al. 68Ga-DOTATOC PET/CT-Based Radiomic Analysis and PRRT Outcome: A Preliminary Evaluation Based on an Exploratory Radiomic Analysis on Two Patients. *Front. Med.* **2021**, *7*, doi:10.3389/fmed.2020.601853.
52. Atkinson, C.; Ganeshan, B.; Endozo, R.; Wan, S.; Aldridge, M.D.; Groves, A.M.; Bomanji, J.B.; Gaze, M.N. Radiomics-Based Texture Analysis of 68Ga-DOTATATE Positron Emission Tomography and Computed Tomography Images as a Prognostic Biomarker in Adults With Neuroendocrine Cancers Treated With 177Lu-DOTATATE. *Front. Oncol.* **2021**, *11*, doi:10.3389/fonc.2021.686235.
53. Laudicella, R.; Comelli, A.; Liberini, V.; Vento, A.; Stefano, A.; Spataro, A.; Crocè, L.; Baldari, S.; Bambaci, M.; Deandreis, D.; et al. [68 Ga]DOTATOC PET/CT Radiomics to Predict the Response in GEP-NETs Undergoing [177 Lu]DOTATOC PRRT: The "Theragnomics" Concept. *Cancers (Basel).* **2022**, *14*, doi:10.3390/cancers14040984.
54. Zwanenburg, A. Radiomics in nuclear medicine: robustness, reproducibility, standardization, and how to avoid data analysis traps and replication crisis. *Eur. J. Nucl. Med. Mol. Imaging* **2019**, *46*, 2638–2655, doi:10.1007/s00259-019-04391-8.
55. Bailly, C.; Bodet-Milin, C.; Couespel, S.; Necib, H.; Kraeber-Bodéré, F.; Ansquer, C.; Carlier, T. Revisiting the Robustness of PET-Based Textural Features in the Context of Multi-Centric Trials. *PLoS One* **2016**, *11*, e0159984, doi:10.1371/journal.pone.0159984.
56. Liberini, V.; De Santi, B.; Rampado, O.; Gallio, E.; Dionisi, B.; Ceci, F.; Polverari, G.; Thuillier, P.; Molinari, F.; Deandreis, D. Impact of segmentation and discretization on radiomic features in 68Ga-DOTA-TOC PET/CT images of neuroendocrine tumor. *EJNMMI Phys.* **2021**, *8*, 21, doi:10.1186/s40658-021-00367-6.
57. Nioche, C.; Orlhac, F.; Boughdad, S.; Reuze, S.; Goya-Outi, J.; Robert, C.; Pellot-Barakat, C.; Soussan, M.; Frouin, F. erique; Buvat, I. Lifex: A freeware for radiomic feature calculation in multimodality imaging to accelerate advances in the characterization of tumor heterogeneity. *Cancer Res.* **2018**, *78*, 4786–4789, doi:10.1158/0008-5472.CAN-18-0125.
58. Hou, J.; Yang, Y.; Chen, N.; Chen, D.; Hu, S. Prognostic Value of Volume-Based Parameters Measured by SSTR PET/CT in Neuroendocrine Tumors: A Systematic Review and Meta-Analysis. *Front. Med.* **2021**, *8*, 771912, doi:10.3389/fmed.2021.771912.
59. Carlsen, E.A.; Johnbeck, C.B.; Loft, M.; Pfeifer, A.; Oturai, P.; Langer, S.W.; Knigge, U.; Ladefoged, C.N.; Kjaer, A. Semi-automatic tumor delineation for evaluation of 64Cu-DOTATATE PET/CT in patients with

neuroendocrine neoplasms: Prognostication based on lowest lesion uptake and total tumor volume. *J. Nucl. Med.* **2021**, *62*, doi:10.2967/jnumed.120.258392.

60. Thuillier, P.; Liberini, V.; Grimaldi, S.; Rampado, O.; Gallio, E.; De Santi, B.; Arvat, E.; Piovesan, A.; Filippi, R.; Abgral, R.; et al. Prognostic value of whole-body PET volumetric parameters extracted from 68Ga-DOTATOC-PET/CT in well-differentiated neuroendocrine tumors. *J. Nucl. Med.* **2022**, *63*, doi:10.2967/jnumed.121.262652.
61. Tirosh, A.; Papadakis, G.Z.; Millo, C.; Hammoud, D.; Sadowski, S.M.; Herscovitch, P.; Pacak, K.; Marx, S.J.; Yang, L.; Nockel, P.; et al. Prognostic Utility of Total 68Ga-DOTATATE-Avid Tumor Volume in Patients With Neuroendocrine Tumors. *Gastroenterology* **2018**, *154*, 998-1008.e1, doi:10.1053/j.gastro.2017.11.008.
62. Toriihara, A.; Baratto, L.; Nobashi, T.; Park, S.; Hatami, N.; Davidzon, G.; Kunz, P.L.; Iagaru, A. Prognostic value of somatostatin receptor expressing tumor volume calculated from 68Ga-DOTATATE PET/CT in patients with well-differentiated neuroendocrine tumors. *Eur. J. Nucl. Med. Mol. Imaging* **2019**, *46*, 2244–2251, doi:10.1007/s00259-019-04455-9.
63. Kim, Y. il; Yoo, C.; Oh, S.J.; Lee, S.J.; Kang, J.; Hwang, H.S.; Hong, S.M.; Ryoo, B.Y.; Ryu, J.S. Tumour-to-liver ratio determined by [68Ga]Ga-DOTA-TOC PET/CT as a prognostic factor of lanreotide efficacy for patients with well-differentiated gastroenteropancreatic-neuroendocrine tumours. *EJNMMI Res.* **2020**, *10*, 63, doi:10.1186/s13550-020-00651-z.
64. Pauwels, E.; Van Binnebeek, S.; Vandecaveye, V.; Baete, K.; Vanbilloen, H.; Koole, M.; Mottaghy, F.M.; Haustermans, K.; Clement, P.M.; Nackaerts, K.; et al. Inflammation-Based Index and 68Ga-DOTATOC PET-Derived Uptake and Volumetric Parameters Predict Outcome in Neuroendocrine Tumor Patients Treated with 90Y-DOTATOC. *J. Nucl. Med.* **2020**, *61*, 1014–1020, doi:10.2967/jnumed.119.236935.
65. Bagci, U.; Yao, J.; Miller-Jaster, K.; Chen, X.; Mollura, D.J. Predicting Future Morphological Changes of Lesions from Radiotracer Uptake in 18F-FDG-PET Images. *PLoS One* **2013**, *8*, doi:10.1371/journal.pone.0057105.
66. Wehrend, J.; Silosky, M.; Xing, F.; Chin, B.B. Automated liver lesion detection in 68Ga DOTATATE PET/CT using a deep fully convolutional neural network. *EJNMMI Res.* **2021**, *11*, doi:10.1186/s13550-021-00839-x.
67. Carlsen, E.A.; Lindholm, K.; Hindsholm, A.; Gæde, M.; Ladefoged, C.N.; Loft, M.; Johnbeck, C.B.; Langer, S.W.; Oturai, P.; Knigge, U.; et al. A convolutional neural network for total tumor segmentation in [64Cu]Cu-DOTATATE PET/CT of patients with neuroendocrine neoplasms. *EJNMMI Res.* **2022**, *12*, doi:10.1186/s13550-022-00901-2.
68. Khan, J.; Rydèn, T.; Van Essen, M.; Svensson, J.; Bernhardt, P. Activity concentration estimation in automated kidney segmentation based on convolution neural network method for 177LU-SPECT/CT kidney dosimetry. *Radiat. Prot. Dosimetry* **2021**, *195*, 164–171, doi:10.1093/rpd/ncab079.
69. Dewaraja, Y.K.; Mirando, D.M.; Peterson, A.; Niedbala, J.; Millet, J.D.; Mikell, J.K.; Frey, K.; Wong, K.K.; Wilderman, S.; Nelson, A.S. A pipeline for automated voxel dosimetry: application in patients with multi-SPECT/CT imaging following 177 Lu peptide receptor radionuclide therapy. *J. Nucl. Med.* **2022**, *63*, jnumed.121.263738, doi:10.2967/jnumed.121.263738.
70. Ding, W.; Yu, J.; Zheng, C.; Fu, P.; Huang, Q.; Feng, D.D.; Yang, Z.; Wahl, R.L.; Zhou, Y. Machine Learning-Based Noninvasive Quantification of Single-Imaging Session Dual-Tracer 18F-FDG and 68Ga-DOTATATE Dynamic PET-CT in Oncology. *IEEE Trans. Med. Imaging* **2022**, *41*, 347–359, doi:10.1109/TMI.2021.3112783.
71. Zwanenburg, A.; Vallières, M.; Abdalah, M.A.; Aerts, H.J.W.L.; Andrearczyk, V.; Apte, A.; Ashrafinia, S.; Bakas, S.; Beukinga, R.J.; Boellaard, R.; et al. The image biomarker standardization initiative: Standardized quantitative radiomics for high-throughput image-based phenotyping. *Radiology* **2020**, *295*, 328–338, doi:10.1148/radiol.2020191145.